Photoinduced electrooptics in the In_2O_3 nanocrystals incorporated into PMMA matrixes

I V Kityk[1], J Ebothe[2], S Tkaczyk[1], R Miedzinski[1], L Nzoghe-Mendome[2], Jibao He[3], Xiangcheng Sun[4], Kai Sun[4], Qingsheng Liu[5], Zhaoyong Sun[5], Jun Lin[6] and Jiye Fang[5]

[1] Institute of Physics, J Dlugosz University Czestochowa, Aleja Armii Krajowej 13/15, Czestochowa, Poland
[2] Laboratoire de Microscopiset d'Etude de Nanstructures, E A N3799, Boite Postale 138, 21, rue Clement Ader, F-51685, Reims, France
[3] Central Instrumental Facilities, Tulane University, New Orleans, LA 70118, USA
[4] College of Engineering, University of Michigan, Ann Arbor, MI 48109, USA
[5] Department of Chemistry, State University of New York at Binghamton, Binghamton, NY 13902-6000, USA
[6] Changchun Institute of Applied Chemistry, Chinese Academy of Sciences, Changchun 130022, People's Republic of China

E-mail: i.kityk@ajd.czest.pl and jfang@binghamton.edu

Abstract

We have observed an appearance of clear morphological structure in composites containing In_2O_3 nanocrystals (NCs) incorporated into polymethyl methacrylite (PMMA) matrices under optical treatment by a polarized femtosecond laser. The initial photoinduced treatment was carried out using a Ti:sapphire femtosecond laser emitting 140 fs p-polarized light at a maximum spectral wavelength 775 nm with pulse repetition 1 kHz. It was found that the average morphological radius is varied maximally only during illumination at liquid helium temperature ($T = 4.2$ K). The morphological average mean radius is strictly dependent on the sizes of incorporated In_2O_3 NCs. Afterwards we measured the linear electrooptic effect at cw He–Ne laser wavelength 633 nm during simultaneous treatment by 1060 and 530 nm coherent beams of a Nd–YAG picosecond laser. We have established that a decrease of the average morphological mean radius favours an increase of the optically poled linear electrooptic coefficient. The diameters of In_2O_3 NCs were evaluated using transmission electron microscopy (TEM) and light-scattering techniques, whereas the NC sizes and morphological average mean radius of formed nanocomposites were estimated by atomic force microscopy (AFM). A relationship between the diameter of the NC, composite morphological mean average radius and effective linear electrooptic coefficient was established.

(Some figures in this article are in colour only in the electronic version)

1. Introduction

Nowadays, many efforts in optical investigations of nanocomposites are directed to the exploration of their optical, particularly luminescent and nonlinear optical, properties described by third-rank polar tensors [1, 2]. However, one of their possible applications may be a study of photoinduced formation of gratings, which substantially modifies the properties including the second-order optical one [3]. It is well known from investigations of bulk semiconducting materials that the illumination by short-time (pico- or femtosecond) laser pulses might lead to the appearance of surface gratings or ripples [4]. This is caused by an interference between the incident and reflected coherent light beams, and the period of the corresponding ripples is usually less than 3/4 of the wavelength of the light [5]. Generally, the observed effect is explained within a framework of photoinduced phonons, particularly anharmonic ones, due to non-centrosymmetry that forms an acentric grating in the medium [6]. In the present work, we studied the influence of external polarized femtosecond laser pulses on the formation of a grating in In_2O_3 NCs incorporated into polymethyl methacrylate (PMMA) and their manifestation in different effects, particularly nonlinear optical ones. After such optical treatment, modification on the nanocomposite surface may occur. This fact is usually neglected during the performance of optical and electronic measurements.

It is necessary to emphasize that the observed phenomenon is in principle different from the mentioned ripple formation [4, 5], because the bulk-like feature is substantially different from the surface-like ones, which are known for the short-time illuminated narrow-gap semiconductors. It is also predicted that incorporation of low-dimensional materials such as NCs into polymer-like matrices may provide additional opportunities for operating by mechanical features of the investigated systems. One of the principal requirements here is to select and deal with large-size nanocrystals [6, 7] (with sizes higher than 10 nm) which combine properties typical for long-range ordered bulk-like compounds and the local nanosized quantum-confined states. It is worth mentioning that the formed grating disappears when the temperature increases to above the glassing temperature for PMMA (equals to ~115 °C) [8].

It is necessary to choose an NC system which generally possesses a mean particle size higher then 10 nm [9, 10]. Here, two of the key parameters are thickness of the reconstructed surfaces and its space homogeneity. It is clear that this layer should possess different total energy (usually higher) compared to the bulk-like long-range ordered crystallites. Accordingly, the corresponding susceptibilities determining all the variety of dielectric constants should also be different. Such reconstructed layers usually possess a thickness varying from 0.5 to 4 nm for the total average diameter of the NC within 10–60 nm. Their size dispersion plays a crucial role for the possibility of their further application as well [9, 10]. It is predicted that various features of nanoquantization should be observed depending on the thickness and grain size. In the case of large dispersion (which usually has taken place), different quantum nanosize levels should substantially destroy the homogeneity. How it was just mentioned a large-size NC possesses a coexistence of long-range ordered phase with the thin surrounding nanosheet with size of 1–3 nm [10]. As a consequence, the coexistence of long-range ordered structure and of typical localized nanosheets (3–5 nm) demonstrates that quantum-confined effects usually exist for NCs with sizes below 10 nm. At the microscopic level, this means a space coexistence of quantum-confined localized states and delocalized band states. Reference [11] describes such interfaces between the NC and its surrounding polymer matrices. Interface regions separating the NC and the surrounding polymers form relatively lower electron density of states with thickness of ~2–5 nm. Such free volumes may be responsible for the observed photoinduced morphology during the coherent optical treatment.
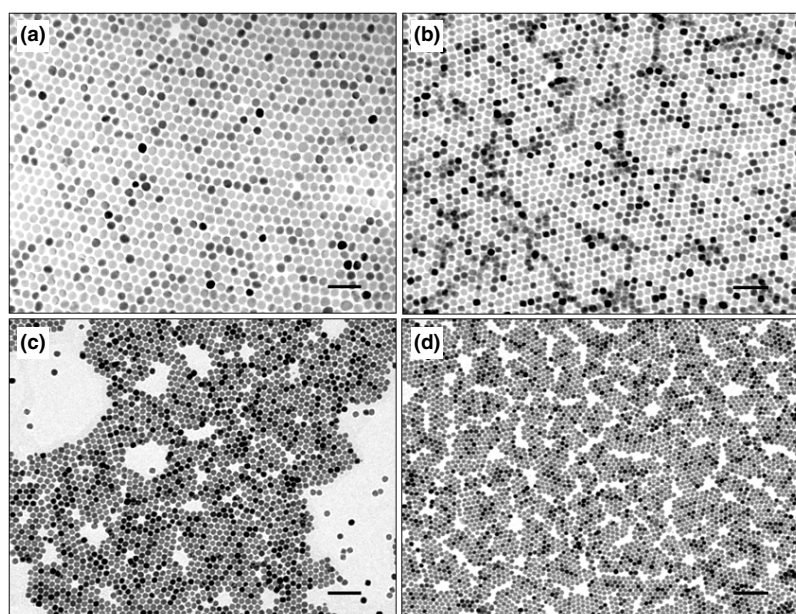
Figure 1. Transmission electron microscopy (TEM) images, recorded from samples (a) **1** (top-left), (b) **2** (top-right), (c) **3** (bottom-left) and (d) **4** (bottom-right). Each bar represents 100 nm.

The NC–polymer system may be also often considered like guest–host nanocomposites [6], in which the NC plays a role of the guest chromophore incorporated into the polymer (glass) host matrix. The relative volume of the boundary regions covering reconstructed NC surfaces and sometimes part of the surrounding disordered background plays a principal role for manifestation of the quantum-confined effects [12]. When the ratio of the reconstructed sheet to the volume is below 0.05, we consider the system as bulk-like crystallites; when this ratio exceeds 0.80, the particles demonstrate substantial nanoquantization, and we treat the system as NCs; whereas all the intermediate systems (between 0.05 and 0.80) are considered as large-size NCs. One of the essential conditions for studying a large-size NC system is a narrow size distribution or high monodispersion, which requires rigorous size and shape controls of the NCs.

2. Experimental section

2.1. Principal parameters of nanocrystallites

In_2O_3 NCs were chemically synthesized by thermally decomposing indium acetate in hexadecane in the presence of oleylamine, oleic acid and trimethylamine N-oxide in appropriate ratio at temperatures as high as 290 °C under an argon stream [13]. The yielded product was isolated by adding a sufficient amount of polar solvent; this was followed by centrifugation. Various sizes of NCs with monodistribution were sorted by performing a standard size-selection operation. Figure 1 presents transmission electron microscopy (TEM) images of four In_2O_3 NC samples, with different average NC sizes, demonstrating high-quality morphology and narrow distribution in size. From these short-range close-packed monolayer patterns, the average diameters for four samples were determined as ∼24 nm (sample indicated **1**), ∼18 nm (**2**), ∼15 nm (**3**) and ∼14 nm (**4**), respectively. The standard deviation of crystalline size for any of the four samples was calculated as no larger than ∼6%.
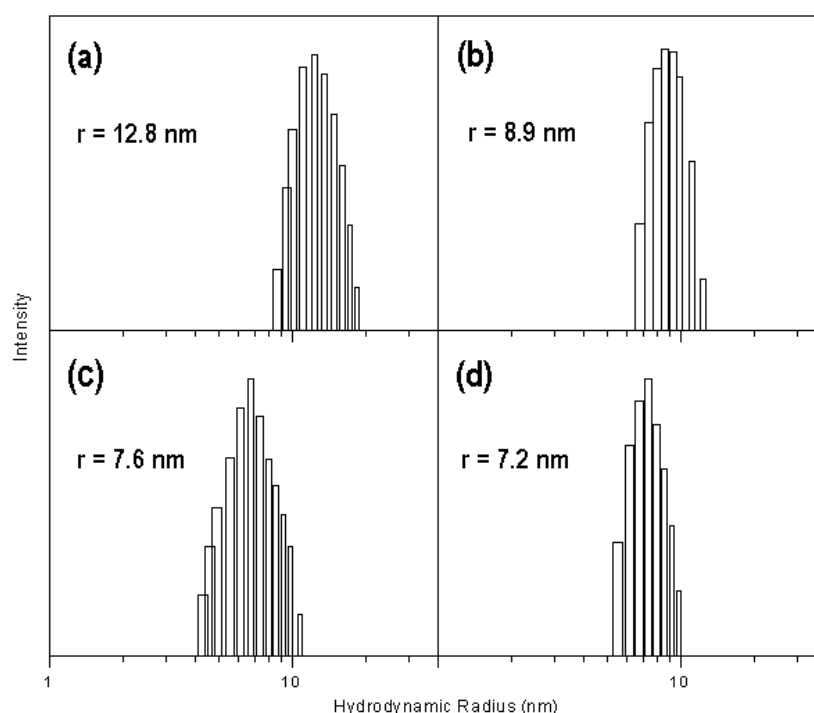
Figure 2. Hydrodynamic radius distribution of samples (a) **1** (∼12.8 nm in radius), (b) **2** (∼8.9 nm in radius), (c) **3** (∼7.6 nm in radius) and (d) **4** (∼7.2 nm in radius).

To verify the size distribution observed from TEM, we have also conducted light-scattering measurements. The light-scattering technique and instruments employed have been described elsewhere (see [11]). Figures 2(a)–(d) illustrate the radius distributions of four In_2O_3 NC samples dispersed in hexane, showing mean hydrodynamic radii of 12.8, 8.9, 7.6 and 7.2 nm, respectively. These results are in a good agreement with those determined from our TEM observation. For all of the In_2O_3 samples, x-ray diffraction (XRD) investigation indicates a cubic phase because all of the detectable diffraction peaks in each pattern are indexed to those from body-centre cubic In_2O_3 (ICDD PDF card No. 06-0416). Based on a calculation using the Scherrer equation [14], the average sizes of crystallites for the four samples were evaluated as 22.9, 17.7, 14.5 and 13.8 nm, which are close to those determined from the TEM observation. As an example, the XRD pattern recorded from sample **1** is revealed in figure 3. A high-resolution TEM image (HRTEM) of sample **2** is presented in figure 4, indicating that the characterized In_2O_3 NCs are highly crystallized, as well as that the TEM-observed NCs are actually truncated octahedral crystals, instead of spherical particles.

To prepare a nanocomposite, 1 g of PMMA was solvated in 5 ml of tetrahydrofuran (THF). Appropriate amounts of In_2O_3 NCs were then incorporated into this solution. Films of such nanocomposite with thickness of 1 μm were deposited on the glass BK7 using a spin-coating technique. The optimal concentration of the NCs was determined as ∼4.5% by weight.

2.2. Femtosecond laser treatment

In order to perform a photoinduced treatment, we chose a femtosecond Ti:sapphire laser system, emitting 140 fs p-polarized light at a maximum spectral wavelength 775 nm with a pulse repetition of 1 kHz. The average beam diameter was varied from 2.6 to 4.1 mm. The
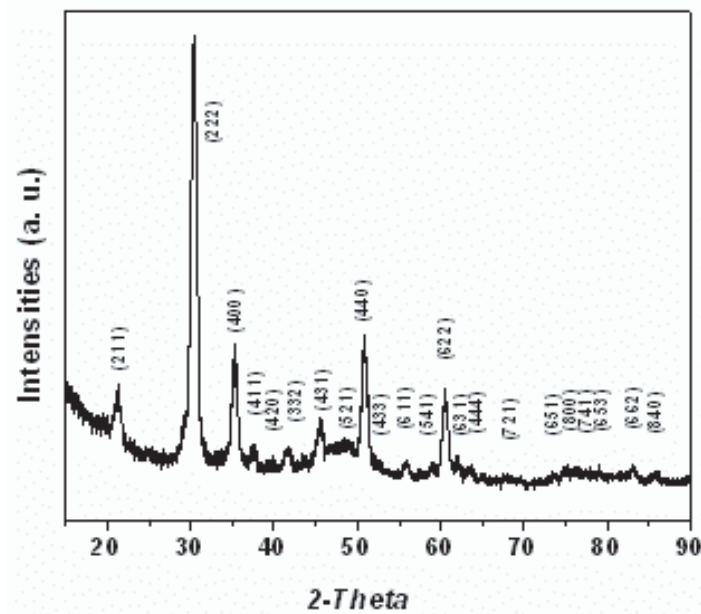
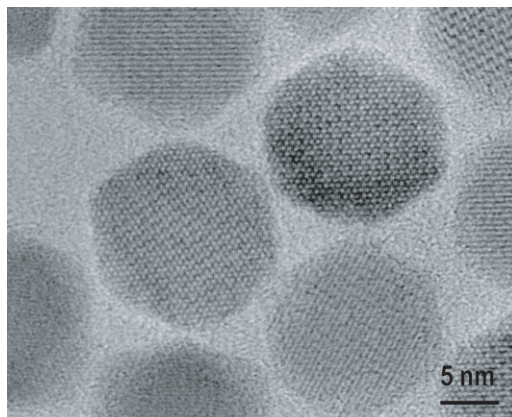**Figure 3.** X-ray powder diffraction pattern of In$_2$O$_3$ NCs (sample **1**).

Figure 4. High-resolution TEM image of In$_2$O$_3$ NCs (sample **2**).

films were placed at position 6 mm away from the focal plane of the focusing lens (focal length $f = 40$ mm). An optically treated beam was directed perpendicular to the surface of the sample. The single-pulse energy was fixed at 30 μJ and the energy density was ~52 mJ cm^{-2}. The number of laser pulses was varied from 100 up to 10^5. To explore the possible photochemical (structural) reaction, we have analysed the changes on surfaces using an x-ray spectroanalyser possessing a monochromatic Al Kα (1486 eV) source and infrared (IR) spectroscopy. No evidence of photodestruction was observed. The performed treatment was done versus temperature and maximal changes of the morphological mean-average radius (determined by TEM and AFM) were observed at liquid helium temperature.
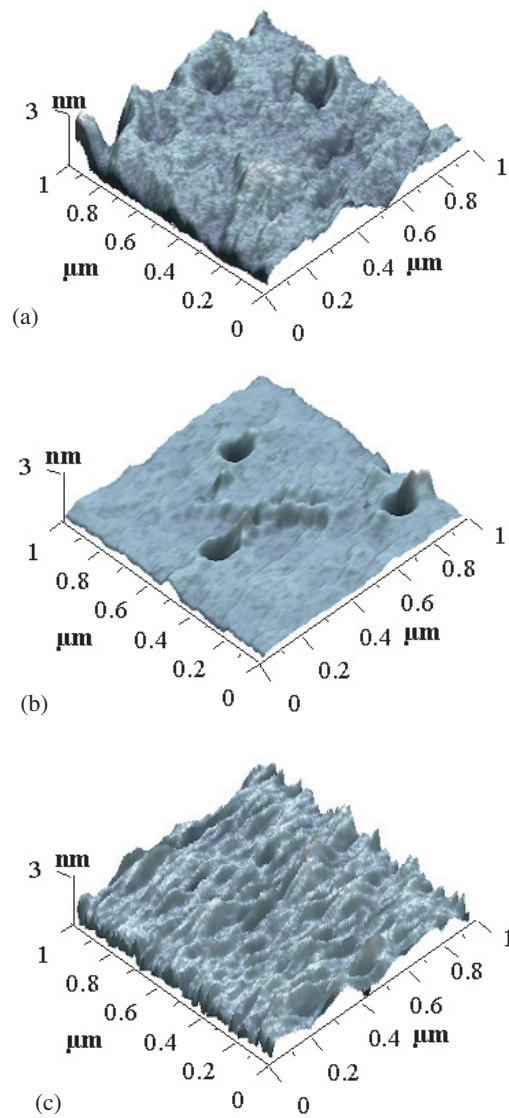
Figure 5. AFM images of the In$_2$O$_3$ NCs (**2**) incorporated into the PMMA; (a) before the femtosecond treatment; (b) after 500 pulses of the femtosecond lasers; (c) after 1500 pulses of the femtosecond lasers.

2.3. AFM monitoring of morphological structure

AFM analyses were performed with a VECCO Nanoscope IIIa operating system in a constant contact force mode. The images were collected in ambient atmosphere, and each of them was digitized into a 512 × 512 pixels with a scanning frequency of ∼1 Hz. The cantilever was made of a commercial Si$_3$Ni$_4$ tip with nearly 20 nm apex radius bearing a spring constant of 0.32 N m^{-1}. The AFM images and average surface profiles of the investigated films composed of PMMA and In$_2$O$_3$ NC sample (sample **2**) are shown in figure 5, clearly revealing the difference in the average morphological radius of the films before and after the femtosecond
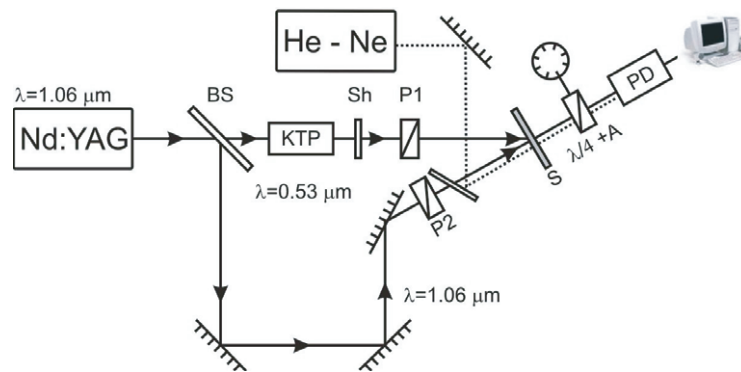
Figure 6. Principal set-up for photoinduced electrooptic measurement.

illumination. These figures confirm the noticeable morphological difference of the films with different embedded NC sizes. We have also established that formation of the fixed average morphological mean radius was achieved just after the 1500–1800 femtosecond laser pulses. The effect was not observed for non-polarized light and for picosecond laser pulses.

2.4. Linear electrooptic effect and optical poling

The linear electrooptic effect is described by a third-rank polar tensor. So to observe such an effect it is necessary to break the centrosymmetry of the medium caused by randomly oriented features of the nanocomposite materials. An efficient method for the formation of non-centrosymmetry in the medium is optical poling, the general principles of which were described in [15–17]. The principle of the method consists in the fact that illumination of isotropic materials by two mutually coherent beams with fundamental and doubled frequencies leads to the formation of long-lived reversible electrostatic polarization of the medium. The illumination of the sample by the two beams is usually called bicolour coherent optical treatment. To be efficient the investigated materials should possess relatively large second- and third-order optical susceptibilities [18]. Besides, the material should possess a relatively large number of trapping centres of different origin, like defects, vacancies, nanoconfined states, etc. The simultaneous optically poled treatment by the two coherent laser beam usually requires from 30–40 s up to several minutes. As a consequence, in the initially randomly oriented medium with the forbidden symmetry for third-rank tensors (to which belong the investigated nanocomposites) there occurs a non-centrosymmetric grating, which may cover both the nanocomposites as well the surrounding medium, like substrates of the nanocomposite films.

A principal set-up for photoinduced electrooptic measurement is shown in figure 6, in which a Nd:YAG laser ($\lambda = 1.06\ \mu$m, 25 ps pulsed) with peak power about 1 MW was used as a fundamental beam for creation of the composite's non-centrosymmetry. The set-up divide the fundamental beam for two channels. The first serves as fundamental ones. Another channel served for the formation of the coherent doubled frequency beam.

Using a beam splitter **BS** and mirror system **M1**–**M3** together with doubled frequency crystal **KTP**, the fundamental laser beam was split into two channels possessing beams with single and double frequencies. The shutter **Sh** was used to switch the channels and to control the scattering background from the fundamental laser beam at 1060 nm. Investigations of the linear electrooptic effect (EOE) or Pockels effects were carried out using a modified dynamic

Senarmont method [19]. As a fundamental probing laser we have applied 633 nm He–Ne laser (with cw power about 6 mW) and spot diameter of ∼600 μm. The specimens were situated between the analyser and phase shifting plate $\lambda/4$ in a diagonal position (i.e. 45° with respect to the crossed polarizer and analyser directions). A sinusoidal AC electric field with a frequency of about 1.3 kHz and maximal amplitude up to 35 V was applied to the top Ag electrodes which were deposited on the substrate with different distances. Having varied the amplitude of the AC voltage, we measured the voltage corresponding to the doubling of the modulated frequency by a lock-in-amplifier. The method allows determining the birefringence with a precision equal to about 8×10^{-6}.

The phototreatment by the two coherent beams was performed at different points on the surfaces in order to avoid possible non-homogeneities in the space distribution of the chromophore.

The pumping and frequency-doubled writing beams were spectrally separated using a grating spectrophotometer (SPM-3) with a spectral resolution about 1 nm mm^{-1}. The photoinduced optical poling experiment consisted of two parts. During the first part (preparation of the grating samples), which took about 3–5 min, the samples were illuminated simultaneously by the fundamental and writing beams. After this time the non-centrosymmetric grating formed was saturated. This saturation was controlled by diffraction of the He–Ne low-power laser beam on the optically formed grating. When the process was saturated we closed the two beams using shutters. During this time we performed measurements of birefringence using the Senarmont scheme. Applying an external electric field, we measured the dependence of the He–Ne laser transparency versus the applied electric field applied perpendicularly to the probing laser beam through the evaporated Ag electrodes. For every sample we changed the distances between the electrodes from 0.3, to 0.6 and 1 mm. Generally the changes of the transparency are described by the equation

$$I = I_0 \sin^2(\pi r_{ijk} U_k d / L\lambda), \tag{1}$$

where I and I_0 are transmitted and incident intensities of the probing He–Ne laser beams with wavelength λ, respectively; d is the film thickness; L is the distance between Ag electrodes. Use of a 1/4 retarded wave-plate allowed us to add additional phase shift, which enhances the sensitivity of the birefringence due to working in the quasi-linear part of the $I = f(U)$ dependences.

The birefringence necessary for determination of the corresponding electrooptic coefficient was evaluated using the equation

$$\Delta n = \lambda \Delta \phi / d, \tag{2}$$

where $\Delta\phi$ is the angle of analyser necessary to obtain the minimum of the transparent light.

It is necessary to add that the value of the birefringence for the surfaces illuminated by the femtosecond laser was at least half an order of magnitude larger compared to the non-illuminated parts.

The corresponding AFM images imply that the morphology of the nanocomposites is greatly dependent on the size of NCs. It is worth emphasizing that the effect for surfaces not illuminated by the femtosecond laser was at least half an order of magnitude less. The morphology and grain size substantially influence the effect observed. Deviations of the NC size in the two directions lead to an increase of the effective photoinduced anisotropic changes, in which the value for the pure PMMA is ∼145 nm. To explain this behaviour, it is necessary to consider the role of interaction between NC interfaces and the surrounding PMMA polymers. It is also worth reporting that the observed morphological average mean radius could be modified only within a certain time of phototreatment by the femtosecond laser pulse. After this period of time, additional laser treatments do not substantially change the morphological
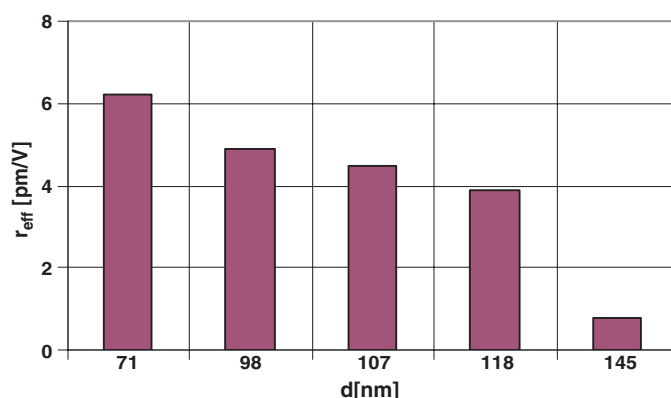
Figure 7. Dependence of the effective electrooptics coefficient versus the effective average mean radius.

Table 1. Principal parameters of the investigated nanocomposites, in which NCs were incorporated into PMMA matrixes with a content of ~4.5% by weight.

NC sizes (nm) and sample identification (in brackets)	Average AFM mean radius of the composites treated by femtosecond laser beams (nm)	Effective electrooptic coefficient (pm V^{-1})
(**4**) 14	118	3.9
(**3**) 15	98	4.9
(**2**) 18	71	6.2
(**1**) 24	107	4.5
PMMA	145	0.8

radius. The grating was formed more clearly with a polarized femtosecond laser, but not with an unpolarized laser. When picosecond laser beams were used, no changes in modulation structure were observed. This might be a consequence of the beam dephasing effect.

Table 1 and figure 7 show a dependences of photoinduced EOE versus NCs of different sizes incorporated into PMMA matrixes. It is clear that minimal average radius and maximal electrooptic coefficient could be achieved when 18 nm NCs were embedded in the PMMA. The data presented unambiguously indicate that 18 nm NCs measured from TEM or 71 nm (in radius) measured using AFM are optimal (give the maximal value of the optically induced EOE).

To understand such behaviour, several assumptions may be proposed. The first is related to the optimal nanointerface thickness touching the PMMA. With the decrease of the morphological average mean radius we have an increase of relative contribution of the near-the-surface nanosheets. The latter due to nanoconfined effects and changes of dielectric susceptibilities may cause a substantial increase of the second-order optical susceptibilities. So the reconstructed layers may substantially change the output electrooptic coefficients. Another possibility is related to modulation of the free volumes on NC/PMMA interfaces. Due to larger electrostatic potentials on the borders separating NCs and the surrounding polymers for samples with lower values of the mean average radius, we deal with the larger third-order susceptibilities. A particular role here is played by the gradients of the electrostatic potentials on the nanocrystallite–polymer borders. Photomechanical stresses which cause additional birefringence and structural non-homogeneities may also be considered as a substantial factor.

The above results demonstrate that the second-order optical effects are very sensitive to the effective sizes of the nanocomposites.

3. Conclusions

With an optical treatment by a femtosecond laser in nanocomposites containing In_2O_3 NCs incorporated into PMMA matrices, we have observed an occurrence of morphological structure with average mean radius determined by the embedded NC sizes. The photoinduced treatment was performed using a femtosecond laser emitting 140 fs p-polarized light at a maximum spectral wavelength 775 nm with pulse repetition 1 kHz. We have established that minimal average morphological mean radius favours maximal photoinduced electrooptic coefficient. A relationship between the diameter of the inorganic NC observed by TEM/light-scattering and the morphological mean radius of nanocomposite estimated by AFM was also discovered. It was established that 18 nm in diameter of In_2O_3 NC corresponds to the average mean radius size of 71 nm in the optically formed morphological structure of the nanocomposite, and the maximally achieved effective electrooptic coefficient value is ~ 6.2 pm V^{-1} (at $\lambda = 633$ nm). This value allows applying the method to the creation of new effective optoelectronic material operated by external femtosecond laser light.

Acknowledgments

References

[1] Kaabi H, Mliki N, Cheynet M, Saikaly W, Gilbert O, Bessaïs B, Yangui B and Charaï A 2006 *Cryst. Res. Technol.* **41** 154–62
[2] Ramos L E, Weissker H-Ch, Furthmüller J and Bechstedt F 2005 *Phys. Status Solidi* b **242** 2977
[3] Yates H M, Pemble M E, Palacios-Lidón E, García-Santamaría F, Rodriguez I, Meseguer F and López C 2005 *Adv. Funct. Mater.* **15** 411–7
[4] Zhou G S, Fauchet P M and Siegman A E 1982 *Phys. Rev.* B **26** 5366
[5] Sipe J E, Young J F, Preston J S and van Driel H M 1983 *Phys. Rev.* B **27** 1141
[6] Jorkaala H and Stennenen H 2002 *J. Opt. A: Pure Appl. Opt.* **4** 366–9
[7] Kityk I V 2001 *J. Non-Cryst. Solids* **292** 184
[8] Konorov S O, Fedotov A B, Ivanov A A, Alfimov M V, Zabotnov S V, Naumov A N, Sidorov-Biryukov D A, Podshivalov A A, Petrov A N and Fornarini L 2003 *Opt. Commun.* **224** 309–20
[9] Kityk I V, Ebothe J, Liu Q, Sun Z and Fang J 2006 *Nanotechnology* **17** 1871–7
[10] Kityk I V 2005 Large-sized nanocrystallites as promising optoelectronic materials *Leading Edge of Semiconductor Physics* (New York: Nova)
[11] Fang J, Stokes K, Wiemann J, Zhou W, Dai J, Chen F and O"Connor C 2001 *Mater. Sci. Eng.* B **83** 254–7
[12] Makowska-Janusik M, Reis H, Papadopoulos M G, Economou I G and Zacharopoulos N 2004 *J. Phys. Chem.* B **108** 588
[13] Liu Q, Lu W, Ma A, Tang J, Lin J and Fang J 2005 *J. Am. Chem. Soc.* **127** 5276
[14] Cullity B D 1978 *Elements of X-ray Diffraction* 2nd edn (Reading, MA: Addison-Wesley)
[15] Osterberg U and Margulis W 1996 *JETP Lett.* **61** 176
[16] Dianov E M, Kazansky P G and Stepanov D Yu 1990 *Sov. J. Quantum Electron.* **17** 926
[17] Antonyuk B P 2000 *Opt. Commun.* **181** 151
[18] Balakirev M K, Kityk I V, Smirnov V A, Vostrikova L I and Ebothe J 2003 *Phys. Rev.* A **67** 023806
[19] Aillerie M, Fontana M D, Abdi F, Carabatos-Nedelec C, Theophanous N and Alexakis G 1989 *J. Appl. Phys.* 2406